

DESY 95-204
November 1995

SOFT INTERACTIONS AT HIGH ENERGY

AHARON LEVY

DESY, Hamburg, Germany
and
Tel-Aviv University, Tel-Aviv, Israel

arXiv:hep-ex/9511006v2 13 Nov 1995

Rapporteur talk given at the International Europhysics Conference on High Energy Physics, Brussels, July 27–Aug 2, 1995

SOFT INTERACTIONS AT HIGH ENERGY

AHARON LEVY

DESY, Hamburg, Germany
and
Tel-Aviv University, Tel-Aviv, Israel

Soft interactions are not easily disentangled from hard ones. In an operational definition of soft and hard processes one finds that at presently analyzed scales there is an interplay of soft and hard processes. As the scale increases, so does the amount of hard processes. So far, nothing is as soft nor as hard as we would like.

1 Introduction

Soft interactions are usually understood as the interactions of hadrons at a relatively small scale. It is sometimes also referred to as low p_T physics, choosing the transverse momenta p_T involved in the process as the representative scale. Clearly this definition is very vague, as the meaning of low p_T is time dependent. We will try to give an operational definition at least for some cases, how one could define more precisely soft and hard interactions.

One could take the approach that anything that can be calculated by pQCD can be called a hard process. All the rest would be soft. The problem however is that what we calculate and what we measure is not the same. In fact, we calculate processes between partons. These 'dress-up' before becoming the colourless object that we measure and thus introduce elements like fragmentation and hadronization which we don't know to calculate in QCD. We thus have an interplay of soft and hard processes, which will be the main motto of this talk.

In the past, hadron-hadron interactions were thought off as the main source of information about soft interactions, while e^+e^- interactions and leptonproduction were traditionally designed to study point-like interactions. The inverse seems to be happening today. The hadron colliders are used for producing the point-like objects while the others provide information on soft phenomena.

The talk will contain two main parts. The first part starts with a short discussion about total cross sections since the bulk of the processes making up the total cross section are believed to be soft interactions. There were however some predictions that the total photoproduction cross section in the HERA energy range will increase sharply due to the resolved part of the photon structure, a prediction which was not borne out by experiment. New results about the photon structure function will be presented from the LEP experiments, which constrain the quarks in the photon.

To learn about the gluon density distribution in the photon one studies jet production at HERA. However, for understanding jets one needs to learn about fragmentation and hadronization and jet shapes. The LEP experiments have submitted very detailed studies about that and about event shapes, particle rates and Bose-Einstein correlations, some of which will be reviewed in this talk.

HERA studies have shown that when viewed from the Breit frame, the current region in ep interactions is very similar to that of e^+e^- reactions, so one can profit from all the studies made at LEP. However the proton side at HERA is still not understood so well. There are indications that much tuning has still to be done in the Monte Carlo generators for a good description of the proton region.

The second part of this talk will be devoted to the interplay between soft and hard interactions by giving some operational definition of soft and hard for the most inclusive (total cross section) and most exclusive (elastic cross section) processes. Are deep inelastic scattering (DIS) processes soft or hard? This question will be discussed by studying the behaviour of the total γ^*p cross section with energy.

One of the surprising results of HERA was the existence of large rapidity gap events in DIS. These showed the behaviour of a diffractive process in which a pomeron is exchanged and which would traditionally be considered as a soft phenomenon. Is that the case also in diffractive reactions in DIS? In a picture where the pomeron is a pseudo particle which contains partons, the Ingelman-Schlein pomeron, the large rapidity gap events in DIS carry information about the structure of the pomeron. Further information about the pomeron can be obtained from exclusive vector meson production in γp and in γ^*p reactions. Does one get a consistent picture from these studies?

Finally, some preliminary evidence for the existence of colour-singlet exchange at high t will be presented.

2 Cross sections

2.1 Total cross section

Donnachie and Landshoff ¹ succeeded to describe all available $\bar{p}p$, pp , $K^\pm p$, $\pi^\pm p$ and γp total cross section values by a simple parametrization of the form $\sigma_{tot} = Xs^{0.0808} + Ys^{-0.4525}$, where s is the square of the total center of mass energy and X and Y are parameters depending on the interacting particles. The value of X is constrained to be the same for particle and antiparticle beams to comply with the Pommeranchuk theorem ². The power of the first term, which in the Regge picture is connected to the intercept of the exchanged pomeron at $t = 0$, ($\alpha_{IP}(0) = 1.08$), was determined by using the $\bar{p}p$ total cross section measurement of E710 ³ at $\sqrt{s} = 1.8$ TeV. CDF ⁴ repeated this measurement at the same \sqrt{s} and found a significantly higher value for the cross section, which would imply a higher pomeron intercept of $\alpha_{IP}(0) = 1.11$. Unfortunately, this discrepancy between the two measurements has not yet been resolved.

Though an ep collider is mainly viewed as a machine to study DIS, the bulk of the neutral current (NC) cross section is in events where the exchanged particle is a photon with a low virtuality Q^2 . By using a calorimeter in the electron direction which measures scattered electrons at very small angles (< 5 mrad), one can tag events produced by photons of virtuality $Q^2 < 0.02$ GeV², with a median Q^2 of 10^{-5} GeV². This way one can study photoproduction reactions of almost real photons at center of mass energies of ~ 200 GeV, which is an order of magnitude higher than was previously available.

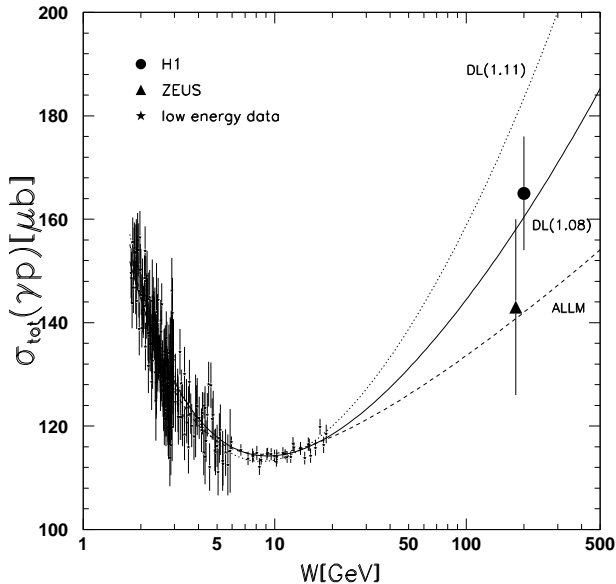


Figure 1: Total photoproduction cross section as a function of the γp center of mass energy W compared to some parametrization, as described in the text.

The H1 ⁵ collaboration submitted a new measurement of the total photoproduction cross section at a γp center of mass energy W of 200 GeV. Their value of $\sigma_{tot}(\gamma p) = 165 \pm 2 \pm 11 \mu b$, plotted in figure 1 together with previous measurements ⁶, agrees well with the value of 1.08 for the pomeron intercept and is lower than that expected from an intercept of 1.11. In addition, this measurement is higher than that expected from the ALLM ⁷ parametrization, to be discussed later.

2.2 Elastic and diffractive cross section

The H1 collaboration measured also cross sections for elastic and diffractive photoproduction processes. In photoproduction reactions, the elastic process is defined through the reactions $\gamma p \rightarrow Vp$, where $V = \rho^0, \omega$, and ϕ . Assuming that the double dissociation cross section is $15 \mu b$, the following results are obtained: $\sigma_{el}(\gamma p) \equiv \sigma(\gamma p \rightarrow Vp) = 17 \pm 4 \mu b$ and $\sigma_{SD}(\gamma p) \equiv \sigma(\gamma p \rightarrow Xp) + \sigma(\gamma p \rightarrow VY) = 32 \pm 12 \mu b$. The single diffraction (SD) processes contain those in which the photon diffracts into a system X and also the process in which the photon turns into one of the three vector mesons ρ^0, ω , or ϕ and the proton diffracts into a system Y . One can then express these results as ratios to the total cross section:

$$\begin{aligned} \frac{\sigma_{el}}{\sigma_{tot}} &= 0.10 \pm 0.03 \\ \frac{\sigma_{SD}}{\sigma_{tot}} &= 0.19 \pm 0.07 \end{aligned} \quad (1)$$

These results are in good agreement with those obtained by the ZEUS ⁶ collaboration at $W = 180$ GeV, which are 0.13 ± 0.05 for the elastic ratio and 0.19 ± 0.04 for the SD ratio.

It is interesting ⁸ to compare these results to a compilation of $\bar{p}p$, pp , Kp , πp cross sections shown in figures 2(a) and 2(b). The ratio of the elastic to total cross section of Kp and πp reactions, wherever available, are smaller than the ratio for $\bar{p}p$ ones, as expected. The γp ratio seems to be smaller than one would naively expect, given the hadronic nature of the photon. On the other hand, from the comparison in figure 2(b), the ratio of single diffractive to total processes seems to be higher than expected. One possible explanation of this fact can be connected to the way one defines the elastic reaction in photoproduction as that of the three lightest vector mesons. Though this might have been reasonable at low energies, it may be underestimating the process at higher energies where the available energy can produce many more vector mesons. Thus, at higher energy one would move some of the cross section contained in the SD to the elastic channel, increasing the elastic ratio and decreasing the single diffractive one.

In spite of this open question of the exact definition of the subprocesses in photoproduction, the total

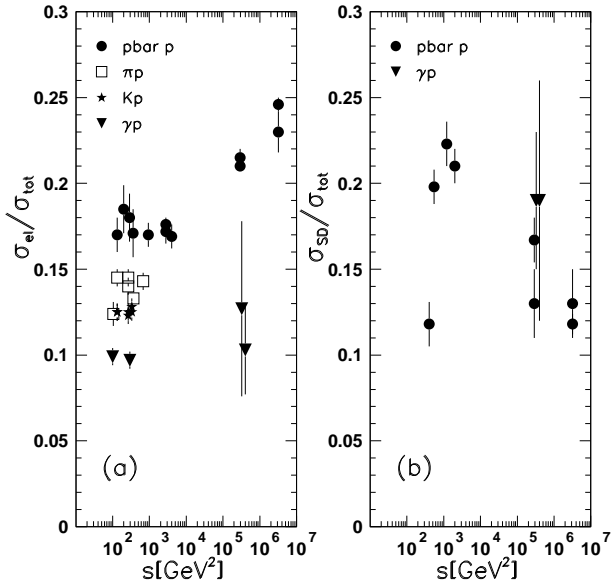


Figure 2: A compilation of the ratio of elastic to total cross section for $\bar{p}p$, Kp , πp and γp reactions as function of the square of the center of mass energy s .

photoproduction cross section has no ambiguity and its energy dependence is in accord with expectations from a soft pomeron phenomenology. It doesn't show the dramatic rise which was predicted by some so-called mini-jet models in which the contribution to the rise comes from the partonic picture of the photon, discussed in the next chapter.

3 The photon structure function

3.1 F_2^γ from e^+e^- reactions

The photon is the elementary gauge particle responsible for electromagnetic interactions. Nevertheless, when interacting with hadrons, it behaves as though it consists of two parts: one in which it acts as a structureless elementary 'bare' photon and a second part in which the photon acts almost like a hadron⁹. Thus one can talk about the notion of the photon structure function and measure it experimentally. It is not exactly like a hadron because the 'structured' part of the photon also consists of two parts: one where the photon acts as a hadronlike object and the process involves non-perturbative effects. This part calls for a treatment similar to that of the proton and is thus denoted as F_2^{HAD} . In the second part, which is unique to the photon, the photon splits into a $q\bar{q}$ pair, and we will denote it by F_2^{box} . This part is also called the point-like part of the photon structure function and can be exactly calculated through the process $\gamma\gamma \rightarrow \gamma\gamma$ described by a box diagram.

For the hadronic part of the photon structure func-

tion one has the same situation as for a regular hadron in the sense that one needs a certain input at a starting scale Q_0^2 . However the hope was that if one can decompose the photon structure function in these two parts

$$F_2^\gamma = F_2^{box} + F_2^{HAD} \quad (2)$$

then by going to high enough Q^2 , $F_2^\gamma \rightarrow F_2^{box}$. Since this part is exactly calculable and depends only on the QCD scale parameter Λ_{QCD} , one could determine the QCD scale parameter by comparing the calculation to the measured structure function.

It was however realized that one can not neglect the hadronic part even at high Q^2 because this part is needed in order to cancel some singularities at small Bjorken x . The situation is not improved by using next to leading order (NLO) calculations. Thus one analyses the photon structure function in a similar way to that of the proton structure function by assuming an input parton distribution at a given scale and evolving to higher scales. Another approach¹⁰ is to use separate inputs for the point-like and the hadronlike components of the photon structure function with a cutoff parameter p_T^0 to separate the two components. A compilation¹¹ of F_2^γ averaged in the region $0.3 < x < 0.8$ can be seen in figure 3.

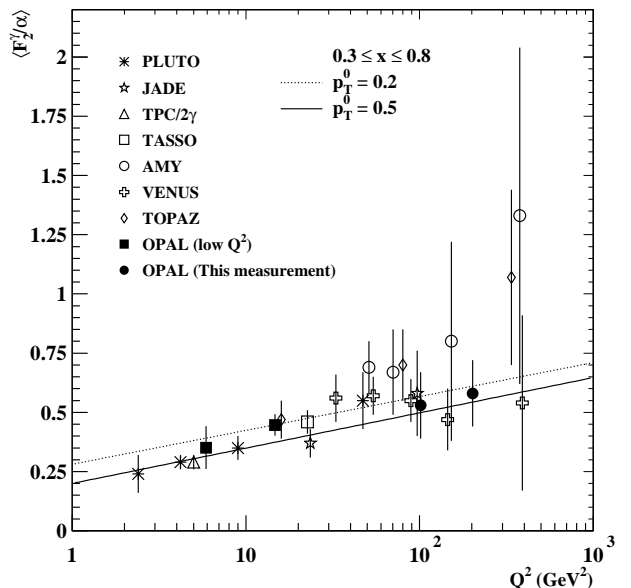


Figure 3: A compilation of the photon structure function averaged in the region $0.3 < x < 0.8$. The lines correspond to two values of the cutoff parameter p_T^0 .

The measurement of the photon structure function is an experimental challenge, especially in the low x region. One has the problem of unfolding the true x distribution from the value of the visible x measured in the detector. This unfolding seems to depend on the models used in the Monte Carlo generators and further studies are needed. The OPAL¹¹ collaboration is currently investigating this

difficulty. The DELPHI¹² collaboration has attempted a measurement of the photon structure function down to the lowest x value published so far, $x = 0.001$. This result, if confirmed, seems to indicate that the structure function does not rise at low x , contrary to the behaviour of the proton structure function.

The different parametrizations of the parton distributions in the photon are all obtained by fitting their expected evolution with Q^2 to the results of the measured F_2^γ . These measurements constrain only the quark distributions in the photon, which is why the gluon distributions are so strongly dependent on which parametrization one uses. In order to constrain also the gluons in the photon one needs to get information from HERA measurements.

3.2 Parton distributions in the photon from HERA

The two components of the photon, the ‘bare’ photon and the photon with structure, are denoted in leading order (LO) by direct photon and resolved photon, respectively, and are depicted in figure 4.

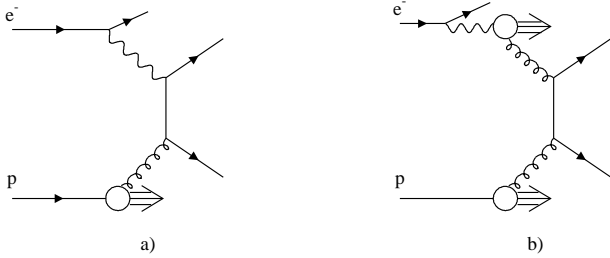


Figure 4: Examples of leading order diagrams for (a) direct and (b) resolved photoproduction.

In diagram (a) the whole momentum of the photon takes part in the reaction with the parton of the proton resulting in two high p_T jets. In diagram (b), only part of the photon momentum participates in the production of the two jets. Denoting by x_γ the fraction of the photon momentum participating in the hard process, one expects $x_\gamma \sim 1$ for the direct photon and $x_\gamma < 1$ for the resolved photon process. One way of estimating x_γ is by defining an observable variable x_γ^{OBS} from the measured high p_T jets which would be a good approximation of the x_γ calculated from the two final state partons:

$$x_\gamma^{OBS} = \frac{E_T^{j1} e^{-\eta^{j1}} + E_T^{j2} e^{-\eta^{j2}}}{2E_\gamma} \quad (3)$$

where E_T is the transverse energy of the jet, η , its pseudo rapidity, and E_γ is the energy carried by the almost real photon. The distribution¹³ of this variable is seen in figure 5. The clear peak at high values of x_γ^{OBS} indicates the presence of direct type processes while the resolved photon processes populate the lower x_γ values.

ZEUS 1993

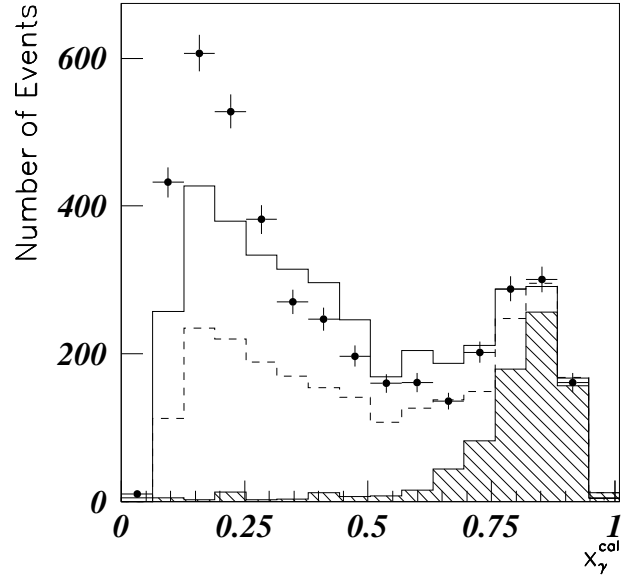


Figure 5: The x_γ distribution. The solid circles are uncorrected ZEUS data. The solid (dashed) line represents the distribution from the PHYTIA (HERWIG) simulation. The LO direct contribution to the HERWIG distribution is shown by the shaded histogram. The Monte Carlo curves have been normalized to fit the direct peak in the data.

The x_γ distribution can in principle be used to extract information about the gluon distribution in the photon. One can assume that the distribution in figure 5 is a sum of the direct and resolved photon processes. By subtracting the estimated direct photon contribution one is left with that coming from the resolved photon processes. This part consists of the contribution from quarks and from gluons. One can estimate the quark part using a parametrization of the quark distribution function as determined from fits to the photon structure function. Thus the difference between the data and the quark es-

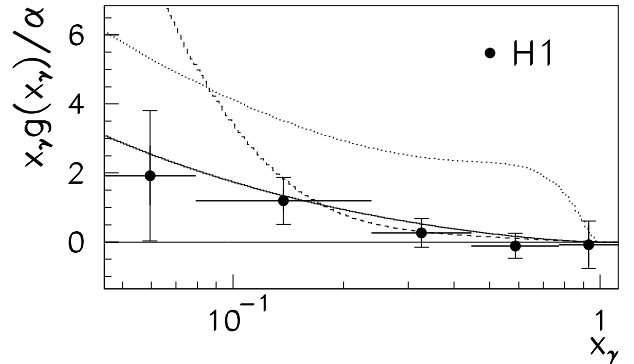


Figure 6: The gluon density distribution in the photon. The data is represented by the solid dots. The lines are expectations from different parametrizations of the gluon distribution in the photon.

timate can be attributed to the gluons in the photon ¹⁴. This difference can be converted into a gluon distribution function of the photon, shown in figure 6. The data are given at a scale of $\langle p_T \rangle^2 = 75 \text{ GeV}^2$. The lines are expectations from different parametrizations of the gluon distribution in the photon.

The method described above gives a rough estimate and a more careful study is planned. However it shows the potential of the high E_T jets measured in the photo-production data of HERA to provide information about the gluons in the photon. The preliminary results given above do not favor a steeply rising gluon distribution at low x_γ predicted by some of the parametrizations.

3.3 Structure of virtual photons

Measurements of the photon structure function has been done so far for real photons. The measurement of x_γ at HERA presented above has been done for almost real photons having virtualities with a median of $10^{-5} - 10^{-3} \text{ GeV}^2$. Do photons of higher virtuality also have structure? The only measurement so far of a structure function of virtual photons has been done more than 10 years ago by the PLUTO ¹⁵ collaboration for a virtuality of 0.35 GeV^2 , showing a slight decrease of the structure function compared to the one for real photons.

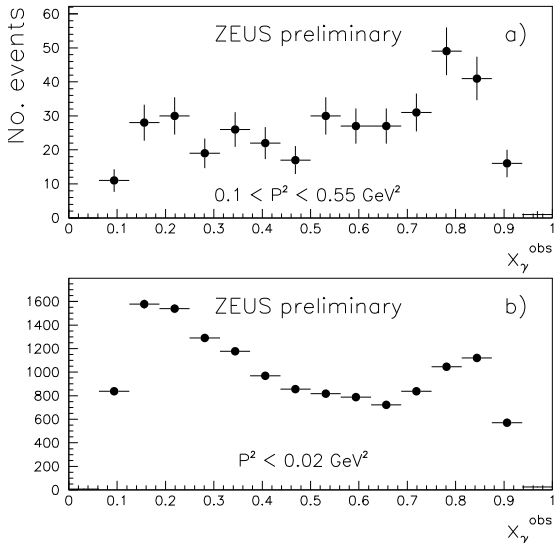


Figure 7: Uncorrected x_γ^{obs} distributions for a) virtual and b) quasi-real photons.

The ZEUS detector implemented a special beam-pipe calorimeter (BPC) which can tag photons of virtuality $0.1 < P^2 < 0.55 \text{ GeV}^2$. In $\gamma\gamma$ physics the virtuality of the target photon is denoted by P^2 and that of the probing photon is denoted by Q^2 . The uncorrected x_γ distribution is shown in figure 7 for the measurements in

the BPC ¹⁶ and compared to the distribution measured in the luminosity electron tagger which measures almost real photons. One sees from figure 7a that in addition to the peak near $x_\gamma^{obs} \sim 1$, which indicates the presence of direct photon processes, there are events also at lower x_γ^{obs} . One thus can conclude that photons of virtuality in the range $0.1 < P^2 < 0.55 \text{ GeV}^2$ also have a resolved part. Furthermore, by making an operational definition of direct photons as those with $x_\gamma^{obs} > 0.75$, one can study the ratio of the resolved to direct photon processes as a function of the photon virtuality P^2 , shown in figure 8. This ratio should not be affected strongly by the acceptance corrections. The ratio of resolved to direct photon

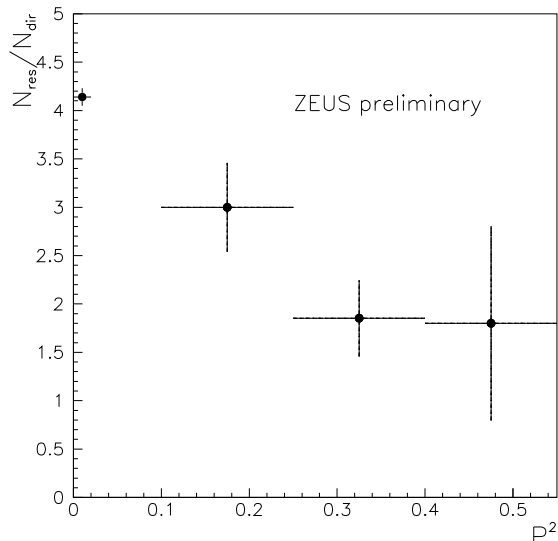


Figure 8: The uncorrected ratio N_{res}/N_{dir} as a function of photon virtuality P^2 (in GeV^2).

processes seems to decrease with increasing photon virtuality in the P^2 range measured here.

The discussion in these last two subsections shows that in order to be able to reconstruct x_γ and thus gain information about parton distributions in the photon at HERA one needs a good understanding of jets. We therefore turn now to the next chapter where we describe the present status of our knowledge about fragmentation and hadronization studies.

4 Fragmentation and hadronization studies

Much of the material in this chapter comes from the LEP experiments and have been covered in the parallel sessions by J.Fuster, W.Metzger, R.Settles, T.Sjöstrand and F.Verbeure. Thus I bring here only a short selection to highlight some points.

4.1 Jet shapes

As was shown in the earlier section, one needs to reconstruct jets in order to get information about the momentum of the partons participating in the hard processes. It is therefore important to have a good understanding of the jet shapes, which are influenced by fragmentation models. Properties of quark jets have been studied for quite some time, thus there is a need to learn more about gluon jets. The DELPHI¹⁷ collaboration presented a study of the energy dependence of the difference between the quark and gluon jet fragmentation. Using quark and gluon jets of purities $\sim 90\%$ they show that gluon jets are broader than quark ones. They measured the charged multiplicity in each as function of the jet energy (figure 9a) and also the dependence of the ratio between the gluon and quark charged multiplicities on the energy (figure 9b). The results were compared with the expectations from the generator JETSET7.3. Not unexpectedly, the description of the gluon jet is not perfect, firstly because it was much less studied and secondly maybe because it has a more complicated colour structure than the quarks. For example, because of QCD coherence, the gluon radiation angle has to be taken into account properly¹⁸.

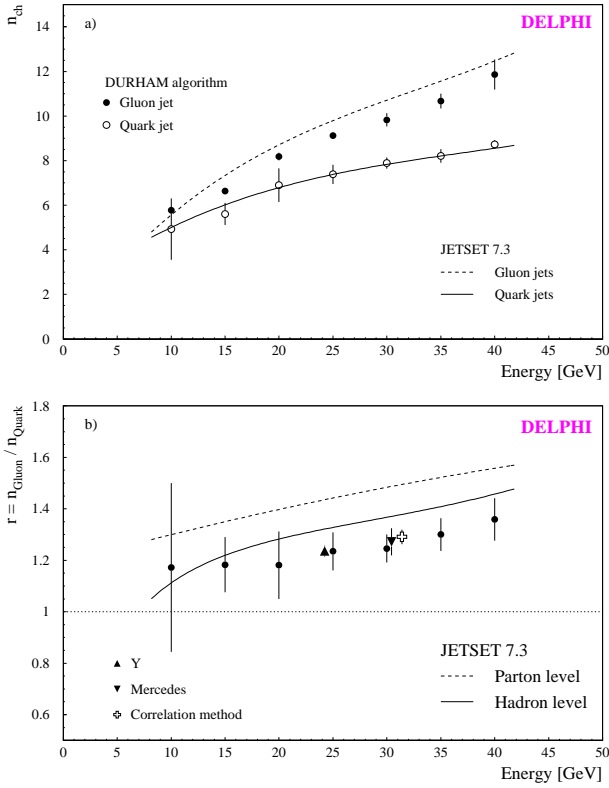


Figure 9: (a) The gluon and quark charged multiplicity distribution as function of the jet energy. (b) The ratio of gluon to quark multiplicities as function of the jet energy.

4.2 Event shapes, particle rates

From jet shapes, we turn to the description of multiparticle final states. The ALEPH¹⁹ collaboration studied the charged multiplicity distribution in different rapidity intervals. They unfolded the data and studied the charged multiplicity in a small rapidity range, a medium range and over the whole rapidity window, as indicated in figure 10. The JETSET7.3 predictions seem to be the only ones which can give a good description of the data in all the rapidity intervals.

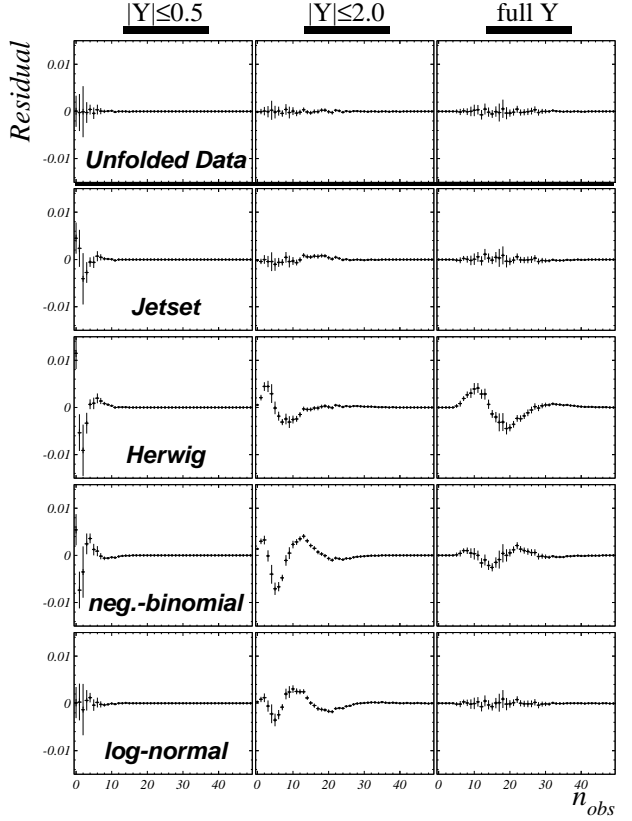


Figure 10: Comparison of charged multiplicity data with unfolded results and with predictions of four models in small, medium and full rapidity range.

It is interesting to check whether the hadronic decomposition of the final state is in agreement with those expected from the generators. One can get the hadrons in the final state either as being formed directly from the string or as decays of more massive hadrons. The OPAL²⁰ collaboration studied the dependence of ξ_{peak} on the hadron mass, where ξ_{peak} is the peak value of the variable $\xi = \ln(1/x_p)$ with x_p being the scaled hadron momentum. As one can see from figure 11 when one includes in addition to the directly produced hadrons also those from the decay of heavier hadrons, the JETSET7.3 Monte Carlo reproduces the pattern observed in the data.

In order to reproduce the rate of inclusive strange particle production, the OPAL collaboration altered the

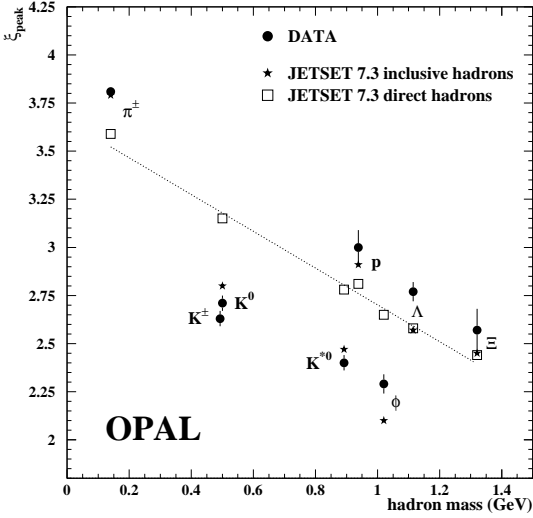


Figure 11: The dependence of ξ_{peak} on the hadron mass, compared to prediction from the JETSET Monte Carlo for direct and inclusive production of particles.

default value of the strangeness suppression factor λ_s from 0.3 to 0.245. The ALEPH ²¹ collaboration finds that it can describe the strange vector meson rate using the default value of $\lambda_s=0.3$. At HERA, both the ZEUS ²² and the H1 ²³ collaborations find that the data are better described with a strangeness suppression value of $\lambda_s \sim 0.2$.

The DELPHI ²⁴ collaboration made a very detailed study of tuning parameters of fragmentation models based on identified particles. They succeed to find parameters which give a good description of most features of the data. The one worrying result is that all models underestimate the tail of the p_T^{out} distribution by more than 25%, where p_T^{out} is the transverse momentum of a particle out of the event plane (see figure 12). From the study of all other variables, the authors conclude that the best overall description is provided by ARIADNE4.06.

Such studies ²⁴ are most useful and should be encouraged since they increase our ability to isolate which of the observations come from fragmentation and which from the underlying basic process.

Can one apply the results obtained at LEP to the HERA physics? There are some clear similarities between e^+e^- and ep reactions. The best way to see that is to compare the e^+e^- results with those of ep obtained in the Breit frame. This is done in figure 13 where the mean charged multiplicity from e^+e^- reactions are compared with twice the mean charged multiplicity of ep reactions ²⁵ in the Breit frame. The results are plotted as function of the photon virtuality in case of ep and for e^+e^- , its center of mass energy. The good agreement between the two reactions indicates that the electron side in ep reactions behaves similarly to that in e^+e^- .

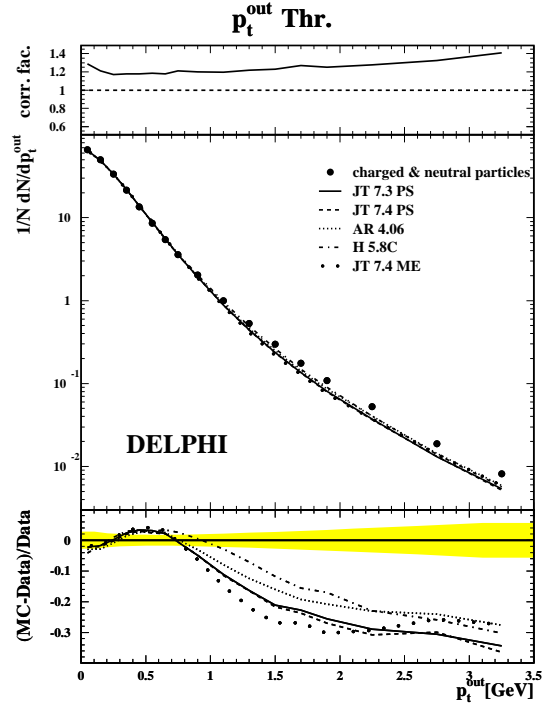


Figure 12: Comparison of p_T^{out} with respect to the Thrust axis with different Monte Carlo models.

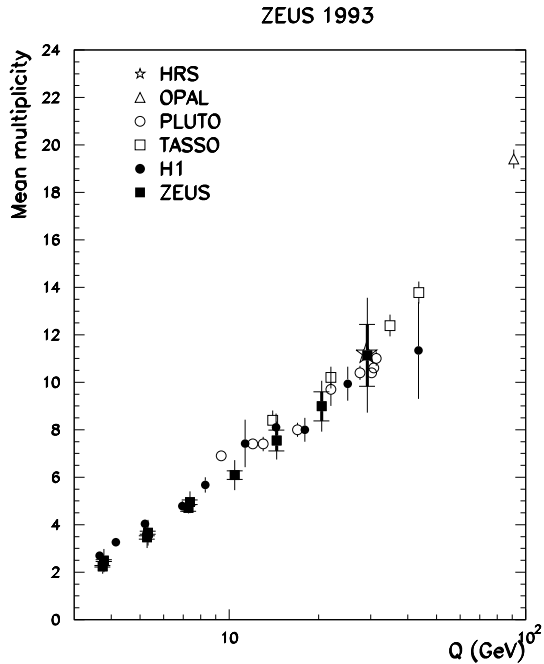


Figure 13: Twice the mean charged multiplicity of ep reactions in the Breit frame compared to the mean charged multiplicity in e^+e^- reactions.

4.3 Multiple interactions

While one could learn about hadronization from e^+e^- reactions as far as the electron side of ep is concerned, the situation at the proton side is different. For very low Q^2 , the quasi-real photon shows structure similar to a hadron. The resolved photon shows a clear spectator structure²⁶ just like in the case of the proton where one has its remnant. One thus can have situations where the remnants of the photon and proton might also interact, thus producing events with multiple interactions²⁷.

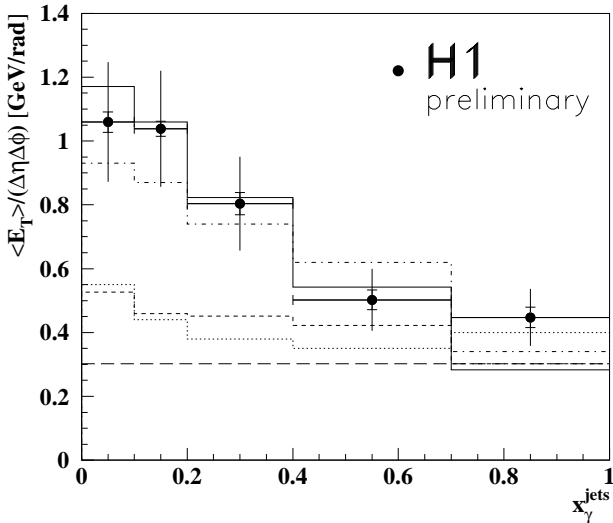


Figure 14: Transverse energy flow outside the two jets as function of x_γ . The histograms which are closer to the data points are MC generators which include multiple interactions, while the lower histograms don't have interactions of the beam remnants.

The H1²⁸ collaboration studied photon proton interactions producing two high E_T jets. They chose the central photon-proton collision region to look for transverse energy flow outside the two jets with the highest E_T . This flow is compared in figure 14 with predictions of Monte Carlo generators with and without the multiple interaction option. This comparison indicated that multiple interactions are needed in order to be able to reproduce the behaviour of the data.

However, this conclusion is not unique. The flexibility of the generators include many more parameters which can be tuned to produce a similar effect to multiple interactions. This is shown by the ZEUS collaboration²⁹ in figure 15, where the uncorrected transverse energy flow around the jet axis is compared with Monte Carlo predictions using different options and different parametrizations of the photon structure function. One can choose a combination of these parameters which does not include multiple interactions and nevertheless get a fair description of the data. It is thus clear that in order to have

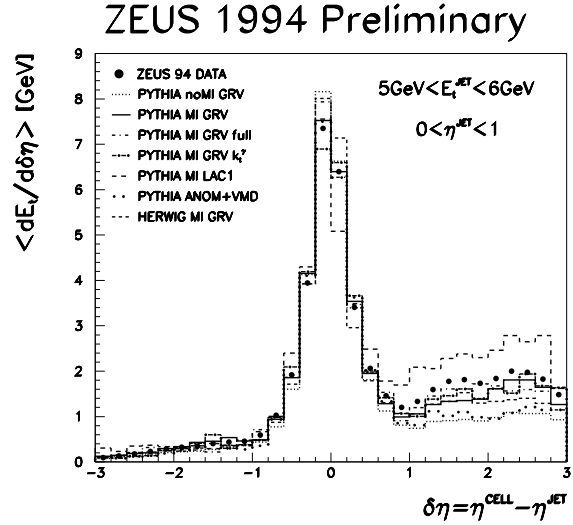


Figure 15: The uncorrected transverse energy flow around the jet axis of jets in the E_T range of 5–6 GeV (dots) compared to predictions of Monte Carlo generators (histograms) using some of the available options.

a better understanding of the fragmentation in the proton region one needs a more detailed study and further tuning of the different generators.

We can summarize this chapter on fragmentation and hadronization studies with the statement that the general features of jet fragmentations, hadronizations, particle multiplicities are quite well described by the generators. One needs much effort to do systematic tuning for finer details. One worrisome problem is that the large p_T distribution of final state hadrons is not properly described. For HERA, the generators need further tuning for the description of the proton side, with a possible sign for multiple interactions.

5 Interplay of soft and hard processes

5.1 Operational definition

It is not completely clear what one means by soft and hard interaction. One would have hoped that by going to the region of DIS one has a better way of probing the hard interactions. As a guideline to help distinguish the two, let us define some operational criteria for what we would consider as a soft and as a hard process. We can not do it in the most general terms, but let us concentrate on some selected measurements: total cross sections and elastic cross sections, the first being the most inclusive and the latter the most exclusive measurement we can make. At high energies, both these processes are dominated by a pomeron exchange.

As discussed earlier, the total $\pi^\pm p, K^\pm p, pp, \bar{p}p$ and

γp cross sections show a slow dependence on the center of mass energy W , consistent with the so-called soft pomeron ¹, having a trajectory

$$\alpha_{IP(\text{soft})} = 1.08 + 0.25t \quad (4)$$

The hard or the perturbative pomeron, also called the Lipatov pomeron or the BFKL ³⁰ pomeron, is expected to have a trajectory

$$\alpha_{IP(\text{hard})} = 1 + \frac{12 \ln 2}{\pi} \alpha_S \quad (5)$$

The definition of the hard IP is quite vague. First, the value of the intercept which is usually taken as 1.5 is a very rough estimate using the expression of the expected power of the reggeized gluon. Using a leading order calculation in $\ln 1/x$, the distribution of the momentum density of the gluon is expected to have the form $xg(x, Q^2) \sim x^{-\lambda}$ where $\lambda = \alpha_S/0.378$. Although usually the value of λ is taken to be 0.5 ³¹, one should note that this requires a value of $\alpha_S = 0.18$, which happens only at large Q^2 , whereas the BFKL calculation is expected to be valid for moderate Q^2 values. The second comment about the assumed hard IP form is the fact that the slope of this trajectory is taken to be zero. The reason for this assumption can be understood intuitively by the fact that the slope is inversely proportional to the average transverse momentum square of hadrons, which is expected to be much larger in hard interactions compared to soft ones.

Following the above definitions of the soft and the hard pomeron, we have some expectations for the behaviour of the total $\gamma^* p$ cross section, $\sigma_{tot}^{\gamma^* p}$, and the elastic one, which in the HERA case is the reaction $\sigma(\gamma^* p \rightarrow Vp)$:

quantity	W dep	soft	hard
$\sigma_{tot}^{\gamma^* p}$	$(W^2)^{\alpha_{IP}(0)-1}$	$(W^2)^{0.08}$	$(W^2)^{0.5}$
slope b of $\frac{d\sigma}{dt}$	$\sim 2\alpha' \ln W^2$	shrink.	no shrink.
$\sigma(\gamma^* p \rightarrow Vp)$	σ_{tot}^2/b	$(W^2)^{0.16}/b$	$(W^2)^1$

We thus turn now to the recent HERA data to check their energy behaviour.

5.2 The total $\gamma^* p$ cross section, $\sigma_{tot}^{\gamma^* p}$

The total $\gamma^* p$ cross section, $\sigma_{tot}^{\gamma^* p}$, can be related to the proton structure function F_2 through the relation

$$F_2(x, Q^2) = \frac{Q^2(1-x)}{4\pi^2\alpha} \frac{Q^2}{Q^2 + 4m_p^2 x^2} \sigma_{tot}^{\gamma^* p}(x, Q^2) \quad (6)$$

where the total $\gamma^* p$ includes both the cross section for the absorption of transverse and of longitudinal photons. In this expression the Hand ³² definition of the flux of virtual photons is used.

DL extended ³³ their parametrization of the total photoproduction cross section also for virtual photons, using however the same energy behaviour as for the real photon case. The ALLM ⁷ parametrization assumed that the power of the energy behaviour, Δ (same meaning as the ϵ used by DL), has a Q^2 dependence with a smooth transition from the value of 0.05 at $Q^2=0$ to ~ 0.4 at high Q^2 . A similar assumption is made also by CKMT ³⁴, who assume a somewhat simpler Q^2 dependence for Δ . Badelek and Kwicinski ³⁵ take a linear combination of generalized vector dominance model (GVDM) and a QCD based calculation, where the weight of each part is Q^2 dependent.

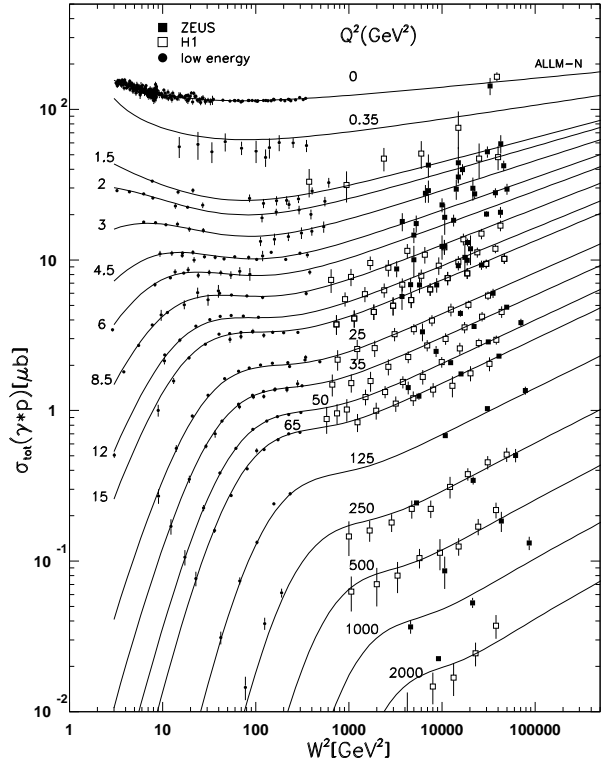


Figure 16: The total $\gamma^* p$ cross section as function of W^2 from the F_2 measurements for different Q^2 values. The lines are the expectations of a new ALLM type parametrization.

Figure 16 presents the dependence of $\sigma_{tot}^{\gamma^* p}$, obtained through equation 6 from the measured F_2 values ^{36,37}, on the square of the center of mass energy, W^2 , for fixed values of the photon virtuality Q^2 . While the data below $Q^2=1$ GeV² show a very mild W dependence, the trend changes as Q^2 increases. Note that for higher values of Q^2 one sees the typical threshold behaviour for the case when $W^2 < Q^2$ ³⁸. The curves are the results of a new ALLM type parametrization which added to the earlier data used in the previous fit data from E665 ³⁹, new data from NMC ⁴⁰ and the published HERA ⁴¹ data.

In order to see how the slope of the W dependence changes with Q^2 , the cross section values in the region

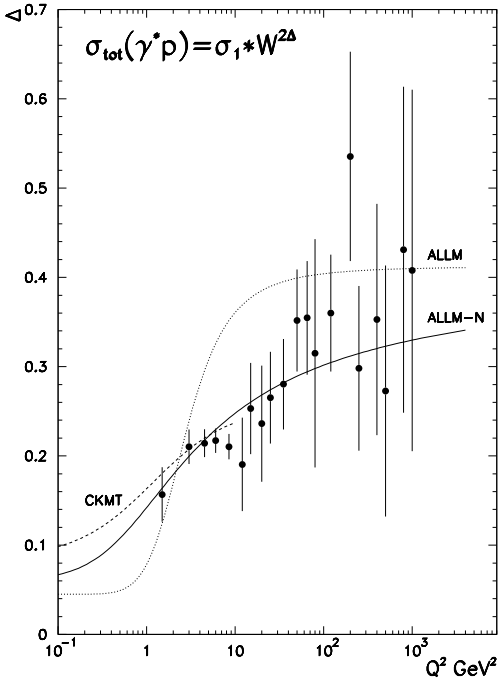


Figure 17: The Q^2 dependence of the parameter Δ obtained from a fit of the expression $\sigma_{tot}^{\gamma^*p} = \sigma_1 W^{2\Delta}$ to the data in each Q^2 bin. The curves are the expectations of the parametrizations mentioned in the text.

where $W^2 \gg Q^2$ were fitted⁴² to the form $\sigma_{tot}^{\gamma^*p} = \sigma_1 W^{2\Delta}$ for each fixed Q^2 interval. The resulting values of Δ from the fit are plotted against Q^2 in figure 17. The curves are the expectations of the CKMT (parametrization valid³⁴ only up to $Q^2 \sim 5-10$ GeV²), the ALLM (fitted without the HERA data) and the updated ALLM-N parametrization, which includes also some of the recent HERA data in its fit. One can see the slow increase of Δ with Q^2 from the value of 0.08 at $Q^2=0$, to around 0.2 for $Q^2 \sim 10-20$ GeV² possibly followed by a further increase to around 0.3-0.4 at high Q^2 . One would clearly profit from more precise data, expected to come soon.

We can thus conclude that the energy behaviour of $\sigma_{tot}^{\gamma^*p}$ indicates that there is a smooth transition from soft to hard interactions with an interplay between the two in the intermediate Q^2 range.

5.3 Vector meson production in γp and in γ^*p

Given the behaviour of the $\sigma_{tot}^{\gamma^*p}$ data, what kind of energy behaviour would one expect for the ‘elastic’ process $\gamma^*p \rightarrow Vp$ for real and virtual photons? In case of photoproduction we have seen that the total cross section follows the expectations of a soft DL type IP . Thus if one takes into account the shrinkage at the HERA energies, one expects $\sigma(\gamma p \rightarrow Vp) \sim W^{0.22}$. In case of DIS production of vector mesons in the range $Q^2 \sim 10-20$ GeV², the expectations are $\sigma(\gamma^*p \rightarrow Vp) \sim W^{0.8}$, since

in this case one expects almost no shrinkage.

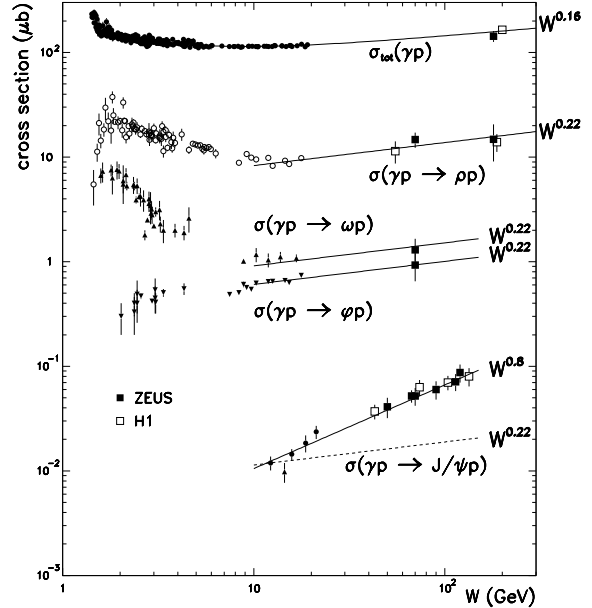


Figure 18: The total and ‘elastic’ vector meson photoproduction measurements as function of W , for the vector mesons ρ , ω , ϕ and J/Ψ . The curve to the total photoproduction cross section is the DL parametrization ($W^{0.16}$). The other lines are curves of the form $W^{0.22}$ and $W^{0.8}$.

Figure 18 presents the measurements of the total and ‘elastic’ vector meson photoproduction cross sections as function of the γp center of mass energy W . As one can see, the high energy measurements of the total and the ρ ^{43,44}, ω and ϕ photoproduction⁴³ follow the expectations of a soft DL type pomeron. However, the cross section for the reaction $\gamma p \rightarrow J/\Psi p$ ^{45,46} rises much faster than the expected $W^{0.22}$ rise from a soft reaction. In fact, it can be well described by a power behaviour of $\sim W^{0.8}$. This surprising behaviour can be understood if one considers the scale which is involved in the interaction. In case of photoproduction reaction, the scale cannot be set by the photon since $Q^2 = 0$. The scale is set by the mass of the vector meson and by the transverse momentum involved in the reaction. Thus, for the lighter vector mesons the scale is still small enough to follow a soft behaviour. However, the mass of the J/Ψ is large enough to produce a scale which would be considered as a hard interaction.

The reaction $\gamma^*p \rightarrow \rho^0 p$ has been measured^{47,48} at two Q^2 values of 8.8 and 16.9 GeV². The reaction $\gamma^*p \rightarrow \phi p$ has been measured⁴⁷ for Q^2 of 8.3 and 14.6 GeV². Since in these cases the scale is set by Q^2 , one expects the energy behaviour to be $\sim W^{0.8}$. The measurements from HERA are compared to the lower energy ones from NMC⁴⁹ and are displayed in figure 19 for the ρ^0 and in figure 20 for the ϕ . In both cases one can see a faster

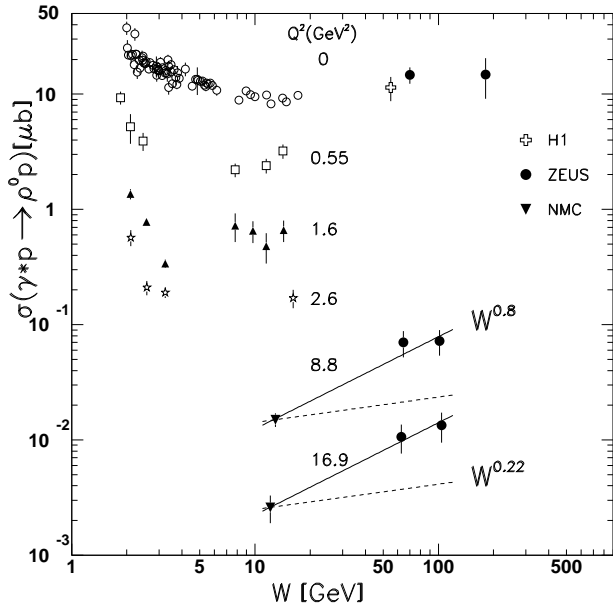


Figure 19: The dependence of the cross section for the reaction $\gamma^*p \rightarrow \rho^0 p$ on W , for different Q^2 values.

rise with W than the soft $W^{0.22}$ behaviour and in good agreement with $W^{0.8}$. These results are thus consistent with the Q^2 dependence of Δ as shown in figure 17.

The ratio of the ϕ to ρ^0 cross sections is expected to be 2:9 according to SU(4). However experimentally this ratio is about 0.07 at $Q^2=0$ ⁵⁰ and increases to about 0.1 at $Q^2 \sim 10$ GeV² in the W range of ~ 10 GeV of the NMC⁴⁹ experiment. The disagreement was explained as a suppression due to the difference in the masses and wavefunctions of the two vector mesons. However, at higher W and higher Q^2 , the effect of these differences are expected⁵¹ to be negligible and the ratio should reach the value of 2/9. One of the interesting questions is whether it is enough to go to higher W or does one need both W and Q^2 to be large.

The ZEUS⁴⁷ collaboration has measured this ratio both at $Q^2=0$ and at $Q^2 \sim 15$ GeV², at a value of $W \sim 100$ GeV. These measurements, together with those of NMC, are plotted in figure 21. It is clear from the figure that in order to reach the expected value of 2/9 one needs both W and Q^2 to be large. One also sees that the value is still not reached, thereby hinting that we still are in the region where the interplay between soft and hard interactions is observed.

Before continuing to the next chapter it is worthwhile to note that the properties observed for vector mesons have a natural explanation in QCD, where vector meson production with a large scale can be described by an exchange mechanism of a pomeron consisting of two gluon. For example, in the case of the model of Brodsky et al.⁵² one expects that the differential ρ^0 cross section produced by longitudinal photons should be proportional

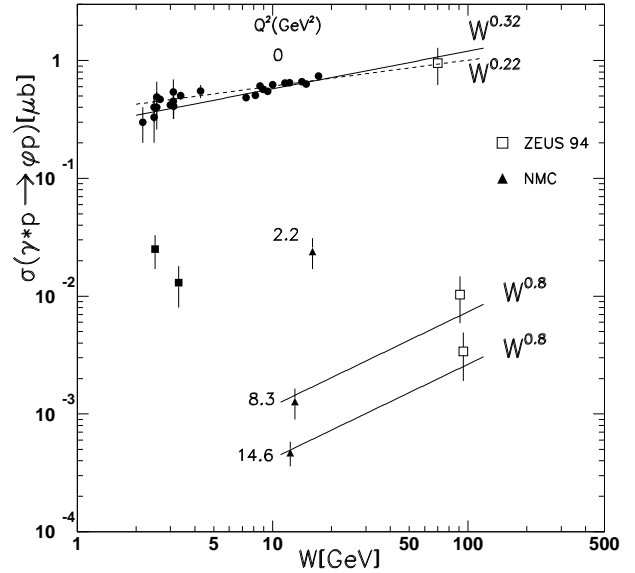


Figure 20: The dependence of the cross section for the reaction $\gamma^*p \rightarrow \phi p$ on W , for different Q^2 values.

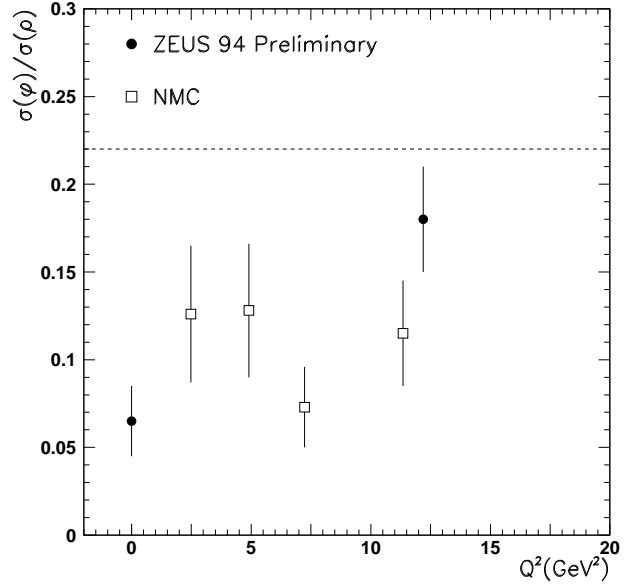


Figure 21: The ratio of the ϕ to ρ^0 cross sections as a function of Q^2 for the ZEUS and NMC data. The dotted line is the expected ratio from SU(4).

to the gluon distribution in the proton:

$$\frac{d\sigma}{dt}(\gamma_L^* p \rightarrow \rho^0 p) \sim \frac{[\alpha_S(Q^2) xg(x, Q^2)]^2}{Q^6} C_\rho \quad (7)$$

Since at low x values $[\alpha_S(Q^2) xg(x, Q^2)]^2 \sim Q$ and since the k_T dependence of the ρ^0 wave function introduces⁵³ another $Q^{0.5}$ dependence, the expectations of the QCD calculation are that the data should have a Q^n dependence, where $n=4.5-5$. The ZEUS⁴⁷ experiment finds $n=4.2 \pm 0.8^{+1.4}_{-0.5}$ and the H1⁴⁸ experimental result is $n=4.8 \pm 0.8$ (statistical error only). The x dependence of the ZEUS⁵⁴ measurement is consistent with their gluon determination from their F_2 measurement.

The conclusion of this chapter is that the reactions $\gamma p \rightarrow Vp$ and $\gamma^* p \rightarrow Vp$ are consistent with the W behaviour of $\sigma_{tot}^{\gamma^* p}$. According to the above operational definition, we observe a transition from soft to hard interactions, with the results in the presently measured kinematic range being driven by an interplay of both.

When a large scale is present, being the virtuality of the photon or the mass of the vector meson, the cross section is consistent with a rise driven by the rise of the gluon momentum density $xg(x, Q^2)$ with W . The pomeron exchange mechanism described by two gluons gives results consistent with the data. In the next chapter we will see what we can say about the structure of the pomeron.

6 Large rapidity gap events in DIS

One of the surprising results of HERA was the discovery^{55,56} of large rapidity gap (LRG) events in DIS processes. These events were shown to be consistent with a picture in which the virtual photon γ^* diffracts into a system with invariant mass M_X , exchanging a colourless object with the properties expected from a pomeron.

In order to understand why this was surprising, consider photoproduction processes. As we saw in chapter 2, about 10% of the total γp cross section comes from processes where the photon diffracts. This hadronic behaviour of the photon is accepted because of the fact that a real photon, which is energetic enough, can fluctuate into a hadronic state before interacting and the fluctuation time is large enough compared to the interaction time so that the hadronic nature of the photon is felt in the interaction. The fluctuation time can be expressed as⁵⁷ $t_f \sim 2E_\gamma/m_V^2$, where E_γ is the photon energy and m_V is the mass of the hadronic state into which the photon fluctuates. The fluctuation time of a virtual photon with virtuality Q^2 is $t_f \sim 2E_\gamma/(m_V^2 + Q^2)$ and thus as the photon virtuality increases, the fluctuation time decreases and the virtual photon behaves like a point-like object. Therefore the generators describing DIS processes did not include diffraction as one of the possible reactions.

However, a closer look at the above argument shows that in fact the diffraction of virtual photons was to be expected. In the region of high W , when $W^2 \gg Q^2$, the fluctuation time can be expressed⁵⁸ as $t_f \sim 1/(m_p x)$. Thus at low x , the fluctuation time is large enough for a virtual photon to diffract like any hadron. The rate

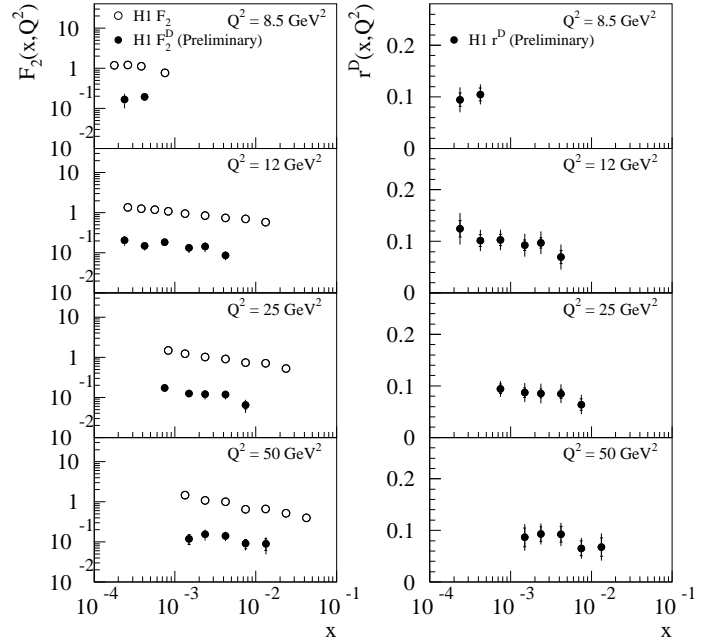


Figure 22: The inclusive structure function (open circles) and the contribution coming from LRG events (full dots) as function of Bjorken x for different Q^2 intervals. In the right part of the figure, the ratio r^D of the two structure function is plotted as function of x for the same Q^2 intervals as in the left part.

of these LRG events is about 10% of the total cross section^{55,56} and is displayed in figure 22 for data of the H1⁵⁹ experiment. The ratio of the LRG events seems to be in first order independent on x and on Q^2 and thus are a leading twist effect.

In order to define a structure function of the LRG events, it is useful to define the following variables in addition to x and Q^2 : the four momentum transfer squared t at the proton vertex, the fraction x_{IP} of the proton momentum carried by the (generic) pomeron emitted by the proton and the fraction β of the pomeron momentum carried by the struck quark. The last two variables can be expressed as:

$$x_{IP} = \frac{M_X^2 + Q^2}{W^2 + Q^2}, \quad \beta = \frac{Q^2}{M_X^2 + Q^2} \quad (8)$$

The three fractional momenta are related by $x = x_{IP}\beta$. Since t is not yet measured by the experiments, one integrates and defines a threefold differential cross section

in the form

$$\frac{d^3\sigma}{d\beta dQ^2 dx_{IP}} = \frac{2\pi\alpha^2}{\beta Q^2} [1 + (1-y)^2] F_2^{D(3)}(\beta, Q^2, x_{IP}) \quad (9)$$

In this expression we have neglected the contribution coming from the longitudinal part of the structure function.

6.1 Factorization

Assuming that the LRG events are produced in a diffractive process where a pomeron is exchanged, it would be interesting to check what are the properties of this exchanged object. Is it an Ingelman–Schlein (IS) ⁶⁰ type of pomeron which behaves similar to a regular hadron? Is it a pomeron as modelled by Nikolaev–Zakharov ⁶¹ by two or more gluon exchanges? In the former case, the $F_2^{D(3)}$ structure function can be factorized into a part which is the flux $f_{IP}(x_{IP})$ of pomerons emitted by the proton, multiplied by the structure function of the pomeron, $F_2^{IP}(\beta, Q^2)$. In the latter case, there is an explicit factorization breaking in the model. Therefore, in order to check the factorization assumption, the measured structure function $F_2^{D(3)}$ was fitted in different β, Q^2 bins to the form

$$F_2^{D(3)} = \left(\frac{1}{x_{IP}}\right)^a C_{\beta, Q^2} \quad (10)$$

where a is kept fixed for all β, Q^2 bins and C is a constant allowed to vary from bin to bin. The form chosen for the flux factor is driven by the Regge phenomenology where one expects the flux of pomerons to have the form

$$f_{IP}(x_{IP}) = \left(\frac{1}{x_{IP}}\right)^{2\alpha_{IP}(t)-1} \quad (11)$$

The measured $F_2^{D(3)}$ by H1 ⁶² and ZEUS ⁶³ are plotted in figure 23 as function of x_{IP} for fixed β, Q^2 bins and fitted to the form expressed in equation 11. The data are consistent with the factorization hypothesis, yielding for the power a of the flux factor the result

$$\begin{aligned} a_{H1} &= 1.19 \pm 0.06 (stat) \pm 0.07 (syst) \\ a_{ZEUS} &= 1.30 \pm 0.08 (stat) \pm_{-0.14}^{0.08} (syst) \end{aligned} \quad (12)$$

The expected power for a DL type soft pomeron would be about 1.10–1.12, depending on the assumed slope of the diffractive peak used in the integration over t and on the value of the slope of the pomeron trajectory. For the case of a hard pomeron as described in the earlier chapter one expects a to be 2. The result is consistent with that of a soft pomeron but also with that of an admixture of both soft and hard pomeron as discussed above. This could be another example of the interplay of soft and hard interactions.

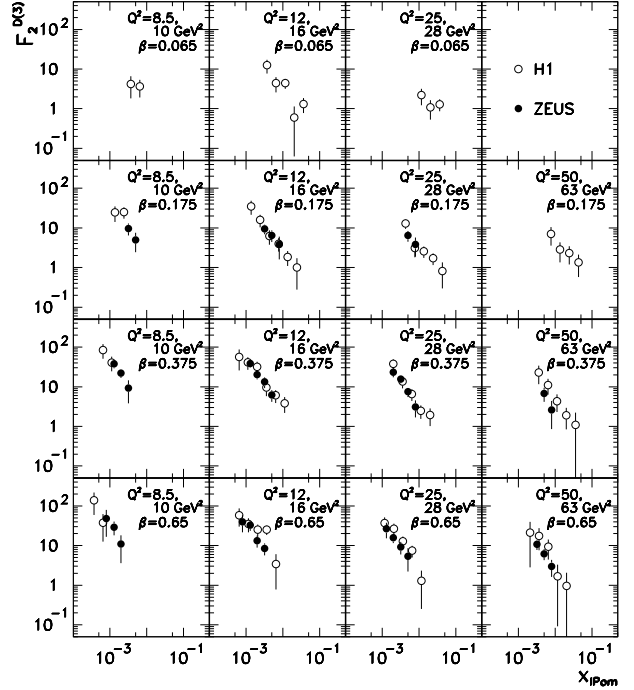


Figure 23: $F_2^{D(3)}(\beta, Q^2, x_{IP})$ as a function of x_{IP} for fixed β, Q^2 bins.

Two notes in passing: (1) though the result is consistent with factorization, it can also be described by the Nikolaev–Zakharov model which assumes factorization breaking. However the breaking in the measured kinematic region is too small to be distinguished by the present accuracy of the data; (2) the behaviour of the data can also be explained by a model like that of Buchmüller and Hebecker ⁶⁴ where the concept of the pomeron is not used and instead assumes a non-perturbative colour cancellation induced by wee partons.

6.2 The structure of the pomeron

If the pomeron has substructure, as postulated by the Ingelman–Schlein model, one could learn about the parton of the pomeron by using the $F_2^{D(3)}$ structure function and compare it to different shapes of parton distribution functions. From the shapes of the distribution of some kinematical variables the HERA experiments found that one needs quarks which have a hard distribution of the form $\beta(1-\beta)$. If in addition one assumes that the partons in the pomeron satisfy a momentum sum rule like a regular hadron, one can get the coefficient of the parton distribution. This is shown in figure 24, where the pomeron is assumed to contain quarks having a hard momentum distribution and the momentum sum rule is assumed to hold. The comparison to the data is done assuming the DL or the IS form for the flux of pomerons. One can see that independent of the assumed flux, the momentum of

the pomeron is not saturated by quarks alone.

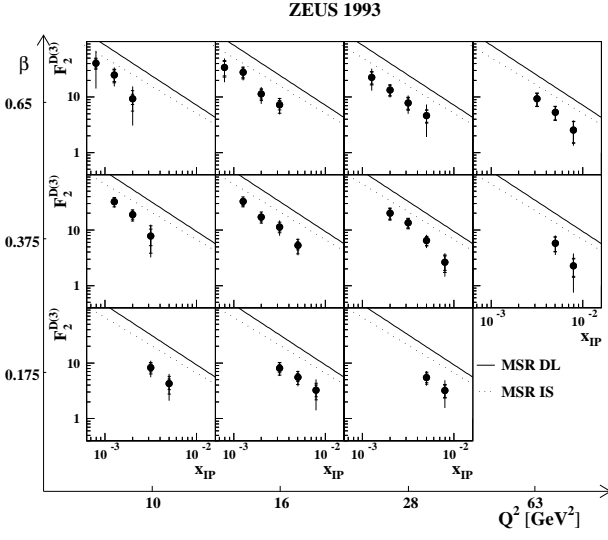


Figure 24: Comparison of the structure function $F_2^{D(3)}$ with the momentum sum rule, using the DL(full line) or the IS(dotted line) flux factors.

Another way of studying the partonic structure of the pomeron is to perform an experiment similar to the two jet production associated with a tagged leading proton experiment carried out by UA8⁶⁵. This was done

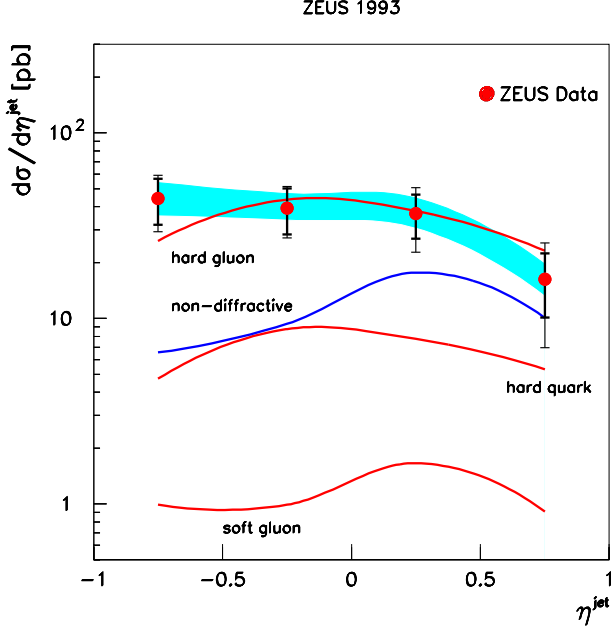


Figure 25: The inclusive jet photoproduction cross section, compared with different parton distributions and with expectations from non-diffractive background, as described in the text.

by ZEUS⁶⁶ which studied large p_T jets photoproduced with a LRG. The cross section values of these events are compared in figure 25 to different parton distributions in

the pomeron, as well as with background coming from non-diffractive events. The flux of the pomeron was assumed to be given by DL and the pomeron was assumed to consist of either only quarks or only gluons, soft or hard, in each case saturating the momentum sum rule. As can be seen from the figure, the data can be explained either by a pure hard gluonic component or by a combination of hard quarks and gluons in the pomeron.

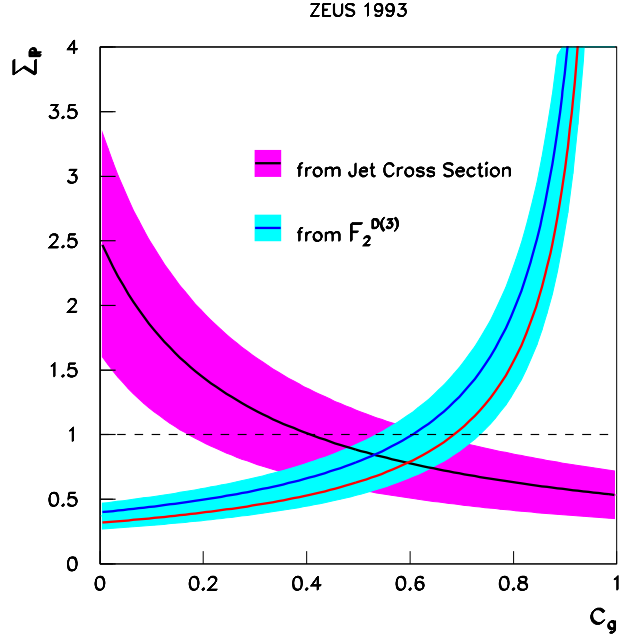


Figure 26: The normalization Σ_{IP} needed to describe the DIS and the photoproduction data as a function of the fraction c_g of gluons in the pomeron.

The conclusions drawn from the comparisons in figure 24 and from those in figure 25, when considered separately, depend on the choice of the pomeron flux and on the assumption of the validity of a sum rule for the pomeron. One can however try and do a comparison based on the joint results of the DIS and the photoproduction data, leaving as free parameters the amount of gluons, c_g , and that of quarks, $1 - c_g$, in the pomeron as well as the overall normalization Σ_{IP} needed to reproduce the results of the two measurements. The region where Σ_{IP} is the same for both determines the amount of gluons in the pomeron in a model independent way, provided the same pomeron is involved in both processes. Such a comparison is shown in figure 26, from which one can conclude that the gluon carries a fraction of $0.3 < c_g < 0.8$ of the pomeron momentum. This result is independent of the assumed expression for the flux, of the validity and of the assumption of a momentum sum rule for the pomeron.

6.3 LRG between jets

Another way of looking for processes where the pomeron is expected to behave differently than the soft pomeron is in large t processes. One possibility is to look for gaps between high p_T jets, which corresponds to a high t two-body reaction. Study of the rate of jets as function of the rapidity gap between the jets can be a source of observing the presence of pomeron exchange in hard processes.

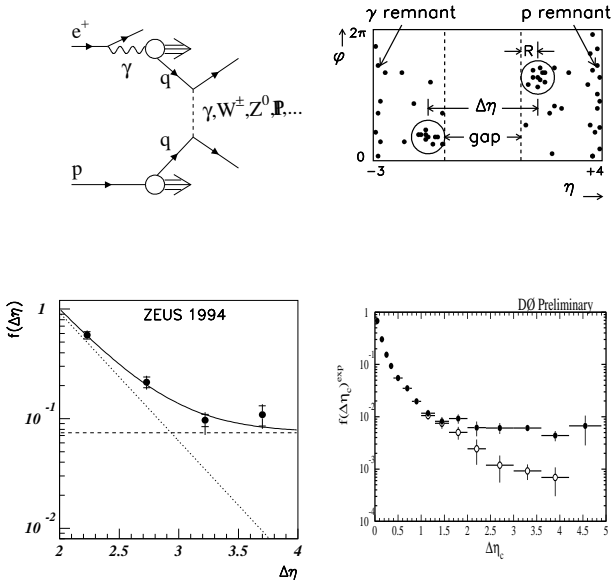


Figure 27: (a) Resolved photoproduction via a colour singlet exchange. (b) The rapidity gap morphology of a two jets event, as described in the text. (c) The gap fraction f as function of the pseudorapidity interval $\Delta\eta$ for the ZEUS data, compared with the result of a fit to an exponential plus a constant. (d) The gap fraction between two jets for the D0 data.

Figure 27(a) describes schematically an example of colour singlet exchange in resolved photoproduction in which a parton in the photon scatters from a parton in the proton, via t -channel exchange of a colour singlet object. The event morphology is described in figure 27(b) where two jets in the final state are shown as circles in (η, ϕ) space and $\Delta\eta$ is defined as the distance in η between the centers of the two jet cones. The gap fraction $f(\Delta\eta)$ for the ZEUS⁶⁷ data are compared in figure 27(c) with the result of a fit to an exponential plus a constant from which one concludes that there is an excess of about 0.07 in the gap fraction over the expectation from colour non-singlet exchange.

There were indeed indications from the CDF⁶⁸ and the D0⁶⁹ collaboration for the existence of rapidity gap between jets at a rate of about 0.01, as shown for the D0 data in figure 27(d). The ZEUS collaboration measurement of 0.07 can be compatible with the Tevatron result if one takes into account the fact that the survival probability of a gap is larger in γp reactions than in $\bar{p}p$ ones.

To conclude this chapter we can say that large rapidity gaps have been observed also in DIS processes. They can be interpreted as being due to diffraction, with the exchange of a pomeron. The diffractive structure function is consistent with the factorization hypothesis in the kinematic range where data exist. In a picture of an Ingelman–Schlein type pomeron with a partonic substructure, a large fraction of the pomeron momentum is carried by gluons. More detailed study is needed before concluding about the soft or hard nature of this pomeron.

There are first signs for the existence of a colour singlet exchange at large t .

7 Summary

One would like to separate soft from hard interactions. However nothing is as soft as we would like nor as hard as we would like. There is an interplay of soft and hard processes at all values of Q^2 . As Q^2 or any other scale increases, the amount of hard processes seems to increase. In order to resolve the hard processes one needs a good understanding of the soft fragmentation and hadronization. By combining various reactions one can try and extract the perturbative QCD part and to learn more about the interplay.

Acknowledgments

I would like to thank H.Abramowicz for her help in preparing this talk and this manuscript. The discussions with L.Frankfurt, E.Gotsman, U.Maor and A.K.Wroblewski were very useful. Thanks also to R.Klanner for a careful reading of this manuscript.

References

- [1] A.Donnachie, P.V.Landshoff, *Phys. Lett.* **296** (1992) 227.
- [2] I.Y.Pomeranchuk, *Sov. Phys. JEPT* **7** (1958) 499.
- [3] E710 Coll., N.A.Amos et al., *Phys. Lett.* **B243** (1990) 158.
- [4] CDF Coll., F.Abe et al., *Phys. Rev.* **D50** (1994) 5550.
- [5] H1 Coll., S.Aid et al., DESY 95–162, submitted to *Zeit. Phys.*
- [6] ZEUS Coll., M.Derrick et al., *Zeit. Phys.* **C63** (1994) 391.
- [7] H.Abramowicz et al., *Phys. Lett.* **B269** (1991) 465.
- [8] E.Gotsman, E.M.Levin, U.Maor, *Zeit. Phys.* **C57** (1993) 677; *Phys. Rev.* **D49** (1994) 4321.
- [9] H.Abramowicz et al., *Int. J. Mod. Phys.* **A8** (1993) 1005.
- [10] J.H.Field, F.Kapusta, L.Poggioli, *Phys. Lett.* **B181** (1986) 362.
- [11] OPAL Coll., Paper EPS–0341, this conference.

- [12] DELPHI Coll., P.Abrew et al., CERN-PPE/95-87, submitted to *Zeit. Phys.*
- [13] ZEUS Coll., M.Derrick et al., *Phys. Lett.* **B354** (1995) 163.
- [14] H1 Coll., T.Ahmed et al., *Nucl. Phys.* **B445** (1995) 195.
- [15] PLUTO Coll., Ch.Berger et al., *Phys. Lett.* **B142** (1984) 119.
- [16] ZEUS Coll., Paper EPS-0384, this conference.
- [17] DELPHI Coll., Paper EPS-0547, this conference.
- [18] Yu. L.Dokshitzer, private communication.
- [19] ALEPH Coll., D. Buskulic et al., CERN-PPE/95-82, submitted to *Zeit. Phys.*
- [20] OPAL Coll., R.Akers et al., CERN-PPE/95-27, submitted to *Zeit. Phys.*
- [21] ALEPH Coll., D. Buskulic et al., CERN-PPE/95-100, submitted to *Zeit. Phys.*
- [22] ZEUS Coll., Paper EPS-0390, this conference.
- [23] H1 Coll., Paper EPS-0479, this conference.
- [24] DELPHI Coll., Paper EPS-0548, this conference.
- [25] ZEUS Coll., M.Derrick et al., *Zeit. Phys.* **C67** (1995) 93; H1 Coll., S.Aid et al., *Nucl. Phys.* **B445** (1995) 3.
- [26] ZEUS Coll., M.Derrick et al., *Phys. Lett.* **B354** (1995) 163.
- [27] T.Sjöstrand, M.vanZijl, *Phys. Rev.* **D36** (1987) 2019.
- [28] H1 Coll., Paper EPS-0476, this conference.
- [29] ZEUS Coll., Paper EPS-0380, this conference.
- [30] E.Kuraev, L.Lipatov, V.Fadin, *Sov. Phys. JEPT* **45** (1977) 199; Ya.Balitskii, L.Lipatov, *Sov. J. Nucl. Phys.* **28** (1978) 822.
- [31] J.C.Collins, J.Kwiecinski, *Nucl. Phys.* **B316** (1989) 307; J.Kwiecinski, A.D.Martin, P.J.Sutton, *Phys. Rev.* **D44** (1991) 2640.
- [32] L.N.Hand, *Phys. Rev.* **129** (1963) 1834.
- [33] A.Donnachie, P.V.Landshoff, *Zeit. Phys.* **C61** (1994) 139.
- [34] A.Capella et al., *Phys. Lett.* **B337** (1994) 358.
- [35] B.Badelek, J.Kwiecinski, *Phys. Lett.* **B295** (1992) 263.
- [36] ZEUS Coll., Paper EPS-0392, this conference.
- [37] H1 Coll., Paper EPS-0470, this conference.
- [38] A.Levy, U.Maor, *Phys. Lett.* **B182** (1986) 108.
- [39] E665 Coll., Preliminary results presented by A.V.Kotwal in *The XXXth Recontres de Moriond, QCD and High Energy Interactions*, March 1995.
- [40] NMC Coll., M.Arneodo et al., CERN-PPE-95-138 (1995).
- [41] ZEUS Coll., M.Derrick et al., *Zeit. Phys.* **C65** (1995) 379; H1 Coll., T.Ahmed et al., *Nucl. Phys.* **B439** (1995) 471.
- [42] H.Abramowicz, A.Levy, in preparation.
- [43] ZEUS Coll., Paper EPS-0389, this conference.
- [44] H1 Coll., Paper EPS-0473, this conference.
- [45] ZEUS Coll., Paper EPS-0386, this conference.
- [46] H1 Coll., Paper EPS-0468, this conference.
- [47] ZEUS Coll., Paper EPS-0397, this conference.
- [48] H1 Coll., Paper EPS-0490, this conference.
- [49] NMC Coll., M.Arneodo et al., *Nucl. Phys.* **B429** (1994) 503.
- [50] T.H.Bauer et al., *Rev. Mod. Phys.* **50** (1978) 261.
- [51] H.Abramowicz, L.Frankfurt, M.Strikman, *Interplay of hard and soft physics in small x deep inelastic processes*, preprint DESY 95-047, 1995.
- [52] S.J.Brodsky et al., *Phys. Rev.* **D50** (1994) 3134.
- [53] L.Frankfurt, W.Koepf, M.Strikman, *Hard diffractive electroproduction of vector mesons in QCD*, preprint TAUP 2290-95, 1995.
- [54] ZEUS Coll., M.Derrick et al., *Phys. Lett.* **356** (1995) 601.
- [55] ZEUS Coll., M.Derrick et al., *Phys. Lett.* **B315** (1993) 481.
- [56] H1 Coll., T.Ahmed et al., *Nucl. Phys.* **B429** (1994) 477.
- [57] B.L.Ioffe, *Phys. Lett.* **30** (1969) 123.
- [58] B.L.Ioffe, V.A.Khoze, L.N.Lipatov, "Hard Processes", North Holland (1984) p. 185.
- [59] H1 Coll., Paper EPS-0491, this conference.
- [60] G.Ingelman, P.Schlein, *Phys. Lett.* **B152** (1985) 256.
- [61] N.N.Nikolaev, B.G.Zakharov, *Zeit. Phys.* **C53** (1992) 331.
- [62] H1 Coll., T.Ahmed et al., *Phys. Lett.* **B348** (1995) 681.
- [63] ZEUS Coll., M.Derrick et al., *Zeit. Phys.* **C68** (1995) 569.
- [64] W.Buchmüller, A.Hebecker, *Phys. Lett.* **B355** (1995) 573.
- [65] UA8 Coll., R. Bonino et al., *Phys. Lett.* **B211** (1988) 239.
- [66] ZEUS Coll., M.Derrick et al., *Phys. Lett.* **B356** (1995) 129.
- [67] Zeus Coll., M.Derrick et al., DESY 95-194, submitted to *Phys. Lett.*
- [68] CDF Coll., F.Abe et al., *Phys. Rev. Lett.* **74** (1995) 855.
- [69] D0 Coll., S.Abachi et al., *Phys. Rev. Lett.* **72** (1994) 2332; Paper EPS-0500, this conference.